

4D Facial Expression Diffusion Model

KAIFENG ZOU, ICube Laboratory, University of Strasbourg, France

SYLVAIN FAISAN, ICube Laboratory, University of Strasbourg, France

BOYANG YU, ICube Laboratory, University of Strasbourg, France

SÉBASTIEN VALETTE, CREATIS, CNRS, INSA-Lyon, Lyon, France, France

HYEWON SEO, ICube Laboratory, University of Strasbourg, France

Facial expression generation is one of the most challenging and long-sought aspects of character animation, with many interesting applications. The challenging task, traditionally having relied heavily on digital craftspersons, remains yet to be explored. In this paper, we introduce a generative framework for generating 3D facial expression sequences (i.e. 4D faces) that can be conditioned on different inputs to animate an arbitrary 3D face mesh. It is composed of two tasks: (1) Learning the generative model that is trained over a set of 3D landmark sequences, and (2) Generating 3D mesh sequences of an input facial mesh driven by the generated landmark sequences. The generative model is based on a Denoising Diffusion Probabilistic Model (DDPM), which has achieved remarkable success in generative tasks of other domains. While it can be trained unconditionally, its reverse process can still be conditioned by various condition signals. This allows us to efficiently develop several downstream tasks involving various conditional generation, by using expression labels, text, partial sequences, or simply a facial geometry. To obtain the full mesh deformation, we then develop a landmark-guided encoder-decoder to apply the geometrical deformation embedded in landmarks on a given facial mesh. Experiments show that our model has learned to generate realistic, quality expressions solely from the dataset of relatively small size, improving over the state-of-the-art methods. Videos and qualitative comparisons with other methods can be found at <https://github.com/ZOUKaifeng/4DFM>. Code and models will be made available upon acceptance.

CCS Concepts: • **Computing methodologies** → Machine learning; Computer graphics.

Additional Key Words and Phrases: diffusion model, neural networks, facial expression, generative model

1 INTRODUCTION

3D facial expression synthesis is a fundamental, long-sought problem in face animation and recognition, with many applications. Due to the inherent subtlety and sophistication of facial expressions, as well as our sensitivity to them, the task is extremely complex. It has traditionally relied on time- and skill-intensive design work by trained artists. The prevailing shape and motion capture technology has changed this paradigm, allowing the algorithmic reconstruction of 3D face shapes and motions of real people. At the same time, its remarkable achievements in the last decades have boosted data-driven approaches to face modeling, which have been succeeded by recent deep learning-based methods. A common strategy is to regress the 3D facial expression of a subject from a 2D video in a frame-by-frame manner[8, 13, 17, 56]. However, such *reconstructive* approach is limited to reproduce facial expressions that have been observed, and requires deformation transfer or animation retargeting to reuse the captured animation of a face to a target face. *Generative* models such as Generative adversarial nets (GANs)[15] and Variational autoencoders (VAEs)[25] can be deployed to the problem of synthesizing realistic yet controllable facial animation that are not limited to a specific observation. However, with a few exceptions[51, 60], most existing works focus on the body motion generation, with various condition signals including text, expression label,

Authors' addresses: Kaifeng Zou, ICube Laboratory, University of Strasbourg, 300 bd Sébastien Brant, Illkirch, France, 67402, kaifeng.zou@unistra.fr; Sylvain Faisan, faisan@unistra.fr, ICube Laboratory, University of Strasbourg, 300 bd Sébastien Brant, Illkirch, France, 6740 frame2; Boyang Yu, ICube Laboratory, University of Strasbourg, 1 Pl. de l'Hôpital, Strasbourg, France, b.yu@unistra.fr; Sébastien Valette, CREATIS, CNRS, INSA-Lyon, Lyon, France, 21 Av. Jean Capelle O, Villeurbanne, France, sebastien.valette@creatis.insa-lyon.fr; Hyewon Seo, ICube Laboratory, University of Strasbourg, 1 Pl. de l'Hôpital, Strasbourg, France, seo@unistra.fr.

or music [16, 27, 28, 39, 54]. This is mainly due to the compact, readily available skeleton-based representation of the body[31], the relatively large set of action vocabulary, and the availability of rich 3D body motion datasets [21, 27, 34, 40, 42]. Unfortunately it is not yet the case with the 3D facial expression.

In this paper, we address the challenging problem of 3D dynamic facial expression generation, one that has not yet received a lot of attention. Most available 3D facial expression datasets [5, 7, 12, 45, 63] come in the form of dense triangular meshes containing thousands of vertices. It is computationally expensive to train a generative model directly using all the vertices. Therefore, similarly to most successful models for 3D facial animation generation, we use a set of predefined 3D face landmarks to represent the dynamics of facial motion. Typically, landmarks are located on facial features that are highly mobile during animation, such as the face outline, eyes, nose, and mouth. The specific aim of the 3D facial animation generation is to learn a model that can generate facial expressions that are realistic, appearance-preserving, rich in diversity, with various ways to condition it such as categorical expression labels. Prior works that have attempted to model the temporal dimension of the face animation [36, 38, 51, 59] mostly leverage auto-regressive approaches, such as Long short-term memory (LSTM) [20] and Gated recurrent units (GRUs) [6]. Here, we propose to use a Denoising Diffusion Probabilistic Model (DDPM) [19, 52, 53], a generative approach that has achieved remarkable success in several domains, such as image generation[44, 48, 50], audio synthesis[26], language modeling[30] and point cloud generation[33]. A DDPM has the nice property of being trainable unconditionally whereas the reverse process can still be conditioned using, a classifier-guidance [10], for instance. This allows us to define the following paradigm: a DDPM is learned unconditionally and several downstream tasks associated with several conditional generations are developed from the same learned model, such as expression control (with label or text), expression filling (with partial sequence(s)), or geometry-adaptive generation (with facial geometry). This makes the proposed approach highly flexible and efficient, benefiting from the generative power of diffusion models while circumventing their limitations of being resource-hungry and difficult to control.

We note that, concurrent to this work, several works have also adopted diffusion models for human motion generation [23, 55, 62]. However, to the best of our knowledge, we are the first to adapt diffusion models to 3D face expression generation. More importantly, although approaches developed in [23, 55, 62] enable different forms of conditioning, they require the diffusion model to be retrained for each way of conditioning.

While the task of 3D facial animation generation has been reduced to the estimation of a temporal sequence of 3D face landmark sets, it is then necessary, in a second task, to compute a sequence of animated meshes. We use an encoder-decoder model similar to [38], which retargets the expression of a 3D face landmark set to the neutral 3D face mesh by computing its per-vertex displacement, in a frame-by-frame manner. Unlike [38], however, we take into account the different morphological shapes of the neutral mesh to adapt the estimation of per-vertex displacements. Results thus obtained validate the effectiveness of the proposed approach.

In summary, our key contributions are as follows: (1) We successfully use a DDPM to propose an original solution to the conditional generation of 3D facial animation. To the best of our knowledge, it is the first to adopt a diffusion-based generative framework in 4D face modeling. (2) We train a DDPM unconditionally and develop several downstream tasks by conditioning the reverse process. In addition to improving the efficiency of training, this paradigm makes the approach highly versatile and easily applicable to other downstream tasks. (3) In various evaluations, the landmark sequence generation and landmark-guided mesh deformation outperform SOTA methods.

2 RELATED WORK

Deep generative models [15, 24, 25, 47, 52] have proven effective at high-quality image synthesis, such as content-preserving image rendering with different styles, and the generation of images depicting learned objects. For 2D images, these models have also shown to be beneficial to facial expression transfer and expression editing tasks. However, the majority of existing solutions address the problem of *static* expression synthesis. Here we review some recent advances achieved in *dynamic* facial expression generation, i.e. modeling and predicting the temporal evolution of poses elicited by facial expressions.

2D facial expression video generation. There is substantial literature addressing the problem of 2D facial expression video generation [3, 36, 57, 60, 61]. MoCoGAN [57] decomposes the video into content and motion: An image-based generator creates the content and GRUs generate the motion. G³AN [60] presents a GAN-based generative model, which also disentangles the appearance and motion of facial video and generates videos by using a spatio-temporal fusion architecture. [59] generates image sequences by using landmark sequences as guidance. Such a landmark-based approach has been also adopted in [36] where a GAN is trained over dynamic facial expressions by deploying manifold-valued representations.

Dynamic 3D facial expression synthesis. To our knowledge, dynamic 3D facial expression synthesis has not been fully explored. [41] synthesizes realistic high resolution facial expressions by using a deep mesh encoder-decoder like architecture to estimate the displacements which are then added to a neutral face frame. [51] deploys LSTMs to estimate the facial landmark changes, which are then used to guide the deformation of a neutral mesh via a Radial Basis Function network. However, both works focus on the displacement estimation for a given expression and do not consider conditional generations. The closest work to ours is Motion3DGAN [38] which extends the aforementioned MotionGAN [36] to model the dynamics of 3D landmarks. The learned distribution of 3D expression dynamics by a WGAN over the hypersphere space is sampled with a condition to generate landmark sequences, which are then fed into a mesh decoder to deform a neutral 3D face mesh frame-by-frame. Our work has several advantages over their work. First, benefiting from the power of diffusion models, we model the input distribution without requiring any extra preprocessing, and can learn from sequences of different lengths. Second, our framework offers a highly versatile and efficient alternative, as we train a DDPM unconditionally and different conditional generations can be performed solely during the reverse process in a plug-and-play manner. Finally, our landmark driven mesh deformation takes into account the identity shape of the input facial mesh and adapt the per-vertex displacements to it, generating a personalized deformation for any given input face.

Given the scarcity of existing work on 3D facial animation generation, we compare our work with some generator models originally dedicated to human motion synthesis, including Action2motion [16] and ACTOR [39].

3 METHOD

At the core of our approach is a DDPM-based model to generate a 3D landmark sequence $x = \{L_1, \dots, L_F\}$ where a frame $L_f \in \mathbb{R}^{N \times 3}$ (for $f = 1$ to F) represents the 3D coordinates of N landmarks. Note that the 3D arrangement of a landmark set L_f implicitly encodes the geometric information specific to the facial anatomy of an individual, and can be viewed as a mixture of the facial identity shape at a neutral pose L and the pose-induced shape change, i.e. $L_f = \Delta L_f + L$. The method is composed of two tasks: First, a DDPM is trained unconditionally (Sec.3.1), whereas conditional

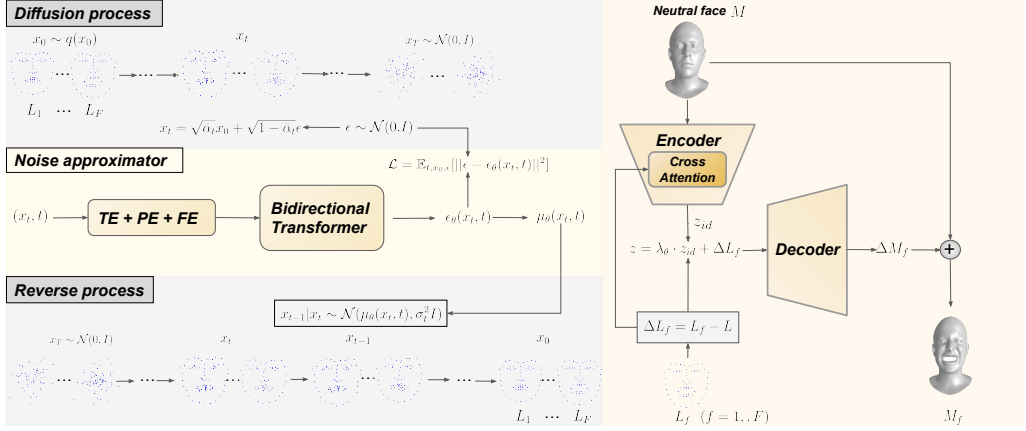


Fig. 1. Overview of the proposed approach. Generally, the diffusion process is used to train the noise approximator while the reverse process is used to sample x_0 from the distribution q . But some tasks developed in Sec. 3.2 require both processes for sampling. The bidirectional transformer takes as input the sum of the outputs of three embedding layers: the temporal embedding layer (TE) that takes as input t , the positional encoding layer (PE) that takes as input an integer sequence from 1 to F , and the feature embedding layer (FE) that takes x_t . The landmark-guided encoder-decoder retargets the expression of L_f onto the input mesh M to estimate M_f at each frame.

generations are obtained by conditioning the reverse process. Different forms of conditioning can be performed, leading to several downstream tasks (Sec.3.2). Then, our landmark-guided encoder-decoder (Sec.3.3) estimates ΔM_f at each frame (for $f = 1$ to F), using a target neutral face mesh M and ΔL_f as input. The desired animation mesh sequence $\{M_1, \dots, M_F\}$ is obtained by adding the estimated displacement ΔM_f to M at each corresponding frame, i.e. $M_f = M + \Delta M_f$. The overview of the proposed method is illustrated in Fig.1.

Note that directly training from and generating full meshes may be beneficial but raises technical issues since the model becomes computationally and memory intensive. An alternative is to utilize diffusion models directly in the latent space of autoencoders [48], or a pre-constructed parameter space of 3D face. Our work can be viewed as akin to the latter approach, except that we use a heuristically defined feature space, i.e., the landmark space, instead of a learned latent space. This choice has been validated by the quality of the reconstruction obtained by the landmark-guided encoder-decoder (Tab. 5).

3.1 Denoising Diffusion Probabilistic Models

DDPMs are latent variable models where the latent variables x_t (for $t = 1$ to T) have the same dimension as the original data $x_0 \sim q(x_0)$. In our work, x_0 is a landmark-based facial animation data: $x_0 = \{L_1, \dots, L_F\}$. Note that it is contrary to most prior works which generate only the displacements ΔL_f [37, 38, 51]. Training our model to generate L_f directly allows it to learn to produce quality expressions that are consistent with the inherent facial morphology.

The joint distribution $p_\theta(x_{0:T})$ from which we derive the likelihood $p_\theta(x_0) = \int p_\theta(x_{0:T}) dx_{1:T}$ is called the reverse process whereas the approximate posterior $q(x_{1:T}|x_0)$ is called the forward process or diffusion process. The diffusion process produces gradually noisier samples (x_1, x_2, \dots, x_T)

by adding Gaussian noise to the initial data x_0 according to a variance schedule β_1, \dots, β_T [19]:

$$q(x_{1:T}|x_0) = \prod_{t=1}^T q(x_t|x_{t-1}) \quad (1)$$

$$q(x_t|x_{t-1}) = \mathcal{N}(x_t; \sqrt{1 - \beta_t}x_{t-1}, \beta_t I). \quad (2)$$

We can derive from Eq. 2 the following property [19] which allows us to train the diffusion model efficiently at an arbitrary time step t :

$$q(x_t|x_0) = \mathcal{N}(x_t; \sqrt{\bar{\alpha}_t}x_0, (1 - \bar{\alpha}_t)I), \quad (3)$$

where $\bar{\alpha}_t = \prod_{s=1}^t \alpha_s$ and $\alpha_t = 1 - \beta_t$.

x_T follows a near-isotropic Gaussian distribution provided that a well-behaved schedule is defined and that T is sufficiently large. DDPM [19] uses this property to sample the target distribution $q(x_0 \sim q(x_0))$. This is achieved by reversing the diffusion process: It begins by sampling x_T from $\mathcal{N}(0, I)$. Next, the reverse process generates progressively less-noisy samples $x_{T-1}, x_{T-2}, \dots, x_1$ until $x_0 \sim q(x_0)$ is obtained, by repeatedly sampling x_{t-1} from $p_\theta(x_{t-1}|x_t)$ by using Eq. 5. This reverse process is formally defined as a Markov chain with learned Gaussian transitions whose mean and variance are estimated by a neural network of parameter θ :

$$p_\theta(x_{0:T}) = p(x_T) \prod_{t=1}^T p_\theta(x_{t-1}|x_t) \quad (4)$$

$$p_\theta(x_{t-1}|x_t) = \mathcal{N}(x_{t-1}; \mu_\theta(x_t, t), \Sigma_\theta(x_t, t)), \quad (5)$$

where $p(x_T) = \mathcal{N}(x_T; 0, I)$. As in [19], we set $\Sigma_\theta(x_t, t)$ to $\sigma_t^2 I$. This is a reasonable choice for generating quality samples, provided that T is chosen to be sufficiently large [35]. Note that estimating $\Sigma_\theta(x_t, t)$ allows sampling with many fewer steps [35].

Several possibilities can be considered to parameterize $\mu_\theta(x_t, t)$ in Eq. 5. [19] shows that approximating the noise ϵ that appears in the following equation:

$$x_t = \sqrt{\bar{\alpha}_t}x_0 + \sqrt{1 - \bar{\alpha}_t}\epsilon, \quad (6)$$

is a suitable choice, especially when combined with a simple loss function (See Eq. 8). Note that Eq. 6 is a different way of writing Eq. 3 ($\epsilon \sim \mathcal{N}(0, I)$). Finally, the term $\mu_\theta(x_t, t)$ can be computed from the approximation of ϵ , denoted as $\epsilon_\theta(x_t, t)$:

$$\mu_\theta(x_t, t) = \frac{1}{\sqrt{\alpha_t}} \left(x_t - \frac{\beta_t}{\sqrt{1 - \bar{\alpha}_t}} \epsilon_\theta(x_t, t) \right). \quad (7)$$

Diffusion models can be trained by optimizing the usual variational bound on negative log-likelihood, but we adopt here the simplified objective function proposed in [19]:

$$\mathbb{E}_{t, x_0, \epsilon} [\|\epsilon - \epsilon_\theta(x_t, t)\|^2], \quad (8)$$

where the term x_t is computed from Eq. 6.

Many previous works [10, 19, 35, 48], especially those for modeling 2D images, have utilized a UNet-like structure[49] to model the mean $\mu_\theta(x, t)$ or the noise $\epsilon_\theta(x, t)$. Here we employ a bidirectional transformer (BiT) [9] to efficiently capture the temporal characteristics of x_t .

3.2 Downstream tasks

The DDPM is learned unconditionally and several downstream tasks are developed from the same learned model, such as expression control (with label or text), expression filling (with partial sequence), or geometry-adaptive generation (with facial geometry). The pseudo code for each task can be found in Appendix D.

Conditioning on expression label (label control). The task is to perform a conditional generation according to the expression label y . Conditioning the reverse process of an unconditional DDPM is achieved by using the classifier-guidance [10, 30, 53]. First, we train a classifier that predicts the label y given a latent variable x_t (and t). Here the classification is conducted with a BiT [9] by adopting the usual approach of adding an extra learnable classification token [9]. Note that the BiT presented here should be distinguished from the other BiT in the diffusion model and is used to condition its reverse process. It is achieved by sampling x_t according to the distribution:

$$p_{\theta, \phi}(x_t | x_{t+1}, y) \propto p_{\theta}(x_t | x_{t+1}) p_{\phi}(y | x_t), \quad (9)$$

where ϕ represents the parameters of the classifier. Sampling of Eq. 9 can be achieved approximately [52] by sampling from a Gaussian distribution similar to the unconditional transition operator $p_{\theta}(x_t | x_{t+1})$, but with its mean shifted by a quantity proportional to $\Sigma_{\theta}(x_t, t) \nabla_{x_t} p_{\phi}(y | x_t)$.

Instead of sampling Eq. 9, we used an alternative way, as proposed in [30]: x_t is computed so as to maximize the \log of Eq. 9. A hyperparameter λ is used to adjust the trade-off between fluency ($p_{\theta}(x_t | x_{t+1})$) and control ($p_{\phi}(y | x_t)$), leading to a stochastic decoding method that balances maximizing and sampling $p_{\theta, \phi}(x_t | x_{t+1}, y)$. As in [30], optimization is achieved by running 3 steps of the Adagrad [11] update for each diffusion step (Alg. 1 of App. D).

Conditioning on text (text control). We also use in this task a BiT guidance, but instead of estimating a label from x_t and t , the BiT outputs a vector of dimension 512 (the softmax layer is removed). As in [54], the BiT is trained so as to increase the cosine similarity between its output and the textual features extracted with CLIP [43] from the text associated with x_0 .

Conditioning the reverse process according to the text c is then achieved (Alg. 2 of App. D) by adapting the procedure presented for the label control: x_t is computed so that it maximizes:

$$\lambda \cdot \log(p_{\theta}(x_t | x_{t+1})) + \cos(\text{BiT}(x_t, t), \text{CLIP}(c)). \quad (10)$$

Conditioning on partial sequence (expression filling). Similarly to inpainting whose purpose is to predict missing pixels of an image using a mask region as a condition, this task aims to predict missing frames of a temporal sequence by leveraging known frames as a condition. The sequence x_0 is composed of F frames, which are either known or unknown. Let \mathcal{S}_K and \mathcal{S}_U denote respectively the set of indices associated with known and unknown frames, and let $x|_{\mathcal{S}}$ denote the subsequence containing only the frames of x whose indices belong to \mathcal{S} .

Since $x_0|_{\mathcal{S}_K}$ is known, note that $x_t|_{\mathcal{S}_K}$ can be drawn according to Eq. 3. Indeed, each component of x_t can be drawn independently since $q(x_t | x_0)$ is an isotropic normal distribution. Sampling from the reverse process conditioned on a partial sequence can also be achieved as follows: x_T is first determined: $x_T|_{\mathcal{S}_U}$ is drawn from $\mathcal{N}(0, I)$ and $x_T|_{\mathcal{S}_K}$ according to Eq. 3. Then, computing x_t from x_{t+1} is achieved in two steps: First, a temporal sequence \hat{x}_t is simply drawn from $p_{\theta}(\cdot | x_{t+1})$ (it is the way to compute x_t in the usual case). $x_t|_{\mathcal{S}_U}$ is set to $\hat{x}_t|_{\mathcal{S}_U}$, while for known frames, $x_t|_{\mathcal{S}_K}$ is directly drawn according to Eq. 3 (Alg. 3 in App. D). Despite its simplicity, this strategy gives satisfactory results as we will demonstrate through qualitative validation in later sections of this paper, provided that the partial sequence is of sufficient length.

Geometry-adaptive generation. Given the facial geometry of a specific subject, a generation can be performed as a special case of expression filling: \mathcal{S}_K is set to $\{1\}$ or to $\{F\}$ (F is the sequence length) and the unique known frame associated with $x_0|_{\mathcal{S}_K}$ is set to the neutral face L of the subject.

The remaining sequence is considered as unknown, for which the model performs an expression filling.

However, we observed that the generated frames may not always smoothly connect to the given frame, a problem that did not arise when the partial sequence remained long enough. In the context of image inpainting, [32] also shows that the simple sampling strategy used for the expression filling task may introduce disharmony. A more sophisticated approach has been proposed so as to harmonize the conditional data $x_t|_{S_K}$ with the generated one $x_t|_{S_U}$ [32]. In order to achieve better convergence properties of the algorithm while maintaining its simplicity, we derive the sequence with five iterations, each with a slight modification: For the first iteration, $x_T|_{S_U}$ is drawn, as previously, from $\mathcal{N}(0, I)$. For the following iterations, $x_T|_{S_U}$, as $x_T|_{S_K}$, is drawn according to Eq. 3 where x_0 is the result obtained from the previous iteration. By doing so, we expect $x_T|_{S_U}$ and $x_T|_{S_K}$ to be harmonized progressively, thus leading to the improved harmonization of $x_t|_{S_U}$ and $x_t|_{S_K}$ along the iterations.

Note that this process can also be easily guided by a classifier (as in the label control) so as to generate a desired facial expression starting from a given facial anatomy (See Alg. 4 in App. D). In this case, the method used for the expression filling must be modified as follows: In the expression filling task, a sequence \hat{x}_t was drawn from $p_\theta(\cdot|x_{t+1})$. In order to guide the reverse process, the sequence \hat{x}_t can now be estimated so as to maximize $\lambda \cdot \log p_\theta(x_t|x_{t+1}) + \log p_\phi(y|x_t, t)$, similarly to the label control case.

3.3 Landmark-guided mesh deformation

To obtain the full mesh sequence $\{M_1, \dots, M_F\}$ from $\{L_1, \dots, L_F\}$, one could use existing fitting methods such as FLAME [29] or DL-3DMM [14] so as to preserve both the facial anatomy and the expression encoded in the landmark frames. However, the meshes generated through the linear blending models tend to lack intricate details of facial geometry, resulting in dull, lifeless shapes. Thus, in our work, we retarget the expression encoded in L_f to the facial geometry given as a (realistic) input mesh M , as in [38]. The mesh M is assumed to be at its neutral pose with a predefined topology [29]. Each mesh frame M_f should retain the facial identity shape M , combined with the expression-driven shape change encoded in $\Delta L_f = L_f - L$ (ΔL_f represents the landmark displacement at f -th frame). This is achieved by our encoder-decoder network that takes both M and ΔL_f as input and predicts ΔM_f at each frame, which is respectively added to M to obtain the final mesh sequence: $M_f = M + \Delta M_f$. This is similar to the Sparse2Dense mesh decoder proposed in [38], except that only ΔL_f (and not M) is used to predict ΔM_f in their work. In our approach, on the other hand, we take into account the different morphological shapes of the neutral mesh M to adapt the estimation of per-vertex displacements ΔM_f .

In order to benefit from the consistent and quality expressions adapted to the facial morphology by the DDPM, one can extract a landmark set L_M from a mesh M , perform the geometry-adaptive task on it to generate a sequence involving L_M , and retarget it to M by the landmark-guided mesh deformation.

Encoder & decoder. Inspired by the Sparse2Dense mesh decoder of [38], we develop an encoder-decoder architecture based on spiral operation layers. The encoder contains a backbone consisting of five spiral operation layers [1] that extracts the features of M . In addition, we propose to incorporate a cross-attention mechanism [58] to account for the possible influence of the characteristics of M on the impact of ΔL_f on each vertex of M : It enables us to find the relevant features of the mesh M that can help predict a latent representation (of ΔM_f) according to ΔL_f . More specifically, the *query* is derived from a linear embedding of ΔL_f (computed by a fully-connected layer FC) and the *key, value* pairs from the output of the backbone (i.e. features of M) denoted as F . The output of the

attention layer writes:

$$\text{softmax} \left(\frac{FC(\Delta L_f) \cdot F^T}{\sqrt{d}} \right) F, \quad (11)$$

where d is the dimension of F . Then a linear layer maps the vector of Eq. 11 to the *identity-aware* representation z_{id} , which is further shifted by the landmark displacement ΔL_f to obtain the final latent representation: $z = \lambda_\theta \cdot z_{id} + \Delta L_f$, where the weight parameter λ_θ is a learnable parameter.

The decoder consists of a linear layer and five spiral operation layers. It takes the latent representation z as input and outputs the per-vertex displacement ΔM_f . M_f is then set to $M + \Delta M_f$. The model is learned using the loss function proposed in [38].

4 EXPERIMENTAL SETTING

As proposed in [19], we set a linear noise schedule starting from $\beta_1 = 1e - 4$ to $\beta_T = 0.02$, and σ_t^2 is set to β_t . T is set to 2000. We train the model on 200K iterations with a learning rate of $1e - 4$ and a batch size of 256. The hyperparameter λ that is used to guide the sampling of the reverse process is set to 0.01 as in [30].

CoMA dataset [46] is a commonly used 4D facial expression dataset in face modeling tasks [2, 22], consisting of over a hundred 3D facial animation sequences captured from 12 subjects, each performing 12 facial actions (“high smile”, “mouth up”, etc.). Each data is composed of a triangular mesh of 5023 vertices undergoing some deformation elicited by an expression.

BU-4DFE dataset [63] contains a total of 606 sequences of 83 landmarks extracted from a sequence of 3D facial scans. Six basic emotional expressions (“anger”, “disgust”, “fear”, “happy”, “sad”, and “surprise”) of 101 subjects have been recorded.

To efficiently capture the essence of expressions while maintaining a small data size, we use 68 landmarks defined by FLAME[29] for both databases. The different sequences have been manually divided into sequences of around 40 frames. Some of them start from the neutral pose and end with a maximal expression intensity (we call them sequences of type N2E), while others evolve from the maximal expression intensity to the neutral face (they are called of type E2N). Since a majority of the methods utilized for comparison necessitate the sequences to share a same length, linear interpolation has been carried out so as to obtain sequences of length 40. Note, however, that our method can deal with sequences of various lengths (See App. B). As a result, our dataset comprises 689 sequences from the CoMA dataset and 1, 212 sequences from the BU-4DFE dataset, totaling 1, 901 sequences with 18 facial actions. Different sequences have been used depending on the specific task at hand. Unless otherwise specified, solely the sequences from the CoMA dataset have been utilized.

5 RESULTS INVOLVING VARIOUS CONDITIONAL GENERATIONS

Here we describe the results we obtained on the various conditional generations. Throughout this section, a classifier that predicts the expression from a sequence independently of its type (see Section 4) is called a classifier of type I (order-**I**nsensitive), whereas a classifier of type S (order-**S**ensitive) predicts both the expression class and the expression type (either N2E or E2N).

For evaluation purposes, an independent classifier (which we denote as IC) is trained to predict the label from a sequence x_0 . We use one LSTM layer followed by a linear layer, as in [38]. The model’s ability to generate a desired expression is assessed by the classification accuracy of the IC tested on the generated expressions. Additionally, the quality of the generated sequence is assessed by using the Frechet Inception Distance (FID) score [18], that compares the distribution of fake data with that of real data. It is computed from the output of the linear layer of the IC.

5.1 Label control

The proposed approach is compared with several SOTA methods which perform conditional sequence generation: Action2Motion [16], Motion3DGAN [38] and ACTOR [39]. The BiT-based classifier used to guide the reverse process, as well as the IC are of type I. Quantitative results as measured by the classification accuracy and the FID score are summarized in Table 1, which confirms that the proposed approach outperforms all SOTA methods. Fig. 2 shows some illustrative results: Our model generates various realistic and quality expressions adapted to various facial geometries. Videos presented in the project website (<https://github.com/ZOUKaifeng/4DFM>) demonstrate the generated expressions, as well as qualitative comparisons among these methods: Sequences generated by our approach are more expressive. The diversity of the generated sequences in terms of both expression and facial anatomy is also illustrated in Appendix C.

Table 1. Performance of different methods for generating desired expressions has been evaluated by measuring the classification accuracy and the FID score. We report as ground truth the FID and the accuracy computed on the test dataset, assuming that an ideal method could have generated it.

| Model | CoMA | | BU-4DFE | |
|--------------|--------|-------|---------|-------|
| | Acc | FID | Acc | FID |
| Ground truth | 83.78% | 2.77 | 99.51% | 6.02 |
| A2M [16] | 52.36% | 29.44 | 80.83% | 19.64 |
| MoGAN [38] | 80.76% | 7.72 | 99.26% | 13.29 |
| ACTOR [39] | 81.40% | 7.11 | 99.13% | 14.56 |
| Ours | 84.97% | 6.79 | 99.89% | 12.37 |

5.2 Text control

To demonstrate this task, we have increased the vocabulary of our dataset by merging CoMA and BU-4DFE. In the first experiment, the raw text label is used to condition the animation (we call it *raw text* task) and the IC used for the evaluation is of type I. In the second experiment, the description of a sequence is enriched to be a short sentence such as “from the neutral face to the raw text label”, or “from the raw text label to the neutral face” (we call it *enriched text* task) and the IC used for the evaluation is of type S.

We compare our results with those of MotionClip [54]. Quantitative results are shown in Table 2. Classification accuracies obtained with the proposed method are slightly higher than those of MotionClip, with FID scores significantly lower. Sequences created by MotionClip are actually realistic but the FID scores are high, due to the lack of diversity in the generated sequences.

Fig. 3 shows illustrative examples obtained with the proposed approach. Note that our model is able to create animated meshes that combine different types of expressions by compositing a text combining different types of expressions. For the complete sequences as well as the qualitative comparisons, readers may refer to the project website.

5.3 Expression filling

Given a partial sequence of an expression, the model can fill up the missing frames. Three experiments have been conducted: In the filling from the beginning (FFB) or the filling from the end (FFE) cases, the length l of the partial sequence is drawn uniformly in [10, 30]. In the filling from



Fig. 2. Animated mesh sequences guided by the label “mouth side” (top), “mouth extreme” (middle), and “cheeks in” (bottom). The meshes are obtained by retargeting the expression of the generated x_0 on different neutral faces.

Table 2. Quantitative evaluation of the text control task. Classification accuracy and FID are computed for the raw text task (rtt, left) and for the enriched text task (ent, right).

| | Acc (rtt) | FID | Acc (ent) | FID |
|--------------|-----------|-------|-----------|-------|
| Ground truth | 86.02% | 3.67 | 74.40% | 4.56 |
| MotionClip | 80.67% | 42.19 | 58.33% | 38.83 |
| Ours | 82.01% | 9.46 | 64.38% | 11.34 |

the middle (FFM) case, l frames have been given at the beginning and at the end of the sequence, respectively. l is uniformly sampled in [5, 15].

The proposed approach for expression sequence filling is compared with a mean imputation strategy. To evaluate the result, an IC (of type I) is trained, so as to check if the filled data has the same expression class as the original one. Results are shown in Table 3. The expression label of the partial sequence is well-captured and reflected in the filled part, leading to an improved classification accuracy especially for the FFM case, where the classification accuracy is comparable to that obtained for the ground truth (Table 1). Classification accuracies obtained in the FFE and FFB cases are lower due to the content of the sequences. As an example, when the partial sequence is associated with the beginning of a sequence of type N2E, it may be composed, at worst, of neutral faces only, or at best of less expressive faces. This is worsened by the fact that sometimes certain expressions appear only at the end of the sequences. This is contrary to the FFM case, where the partial sequence contains both the neutral and the most expressive poses.

Finally, there is a significant improvement of FID score after filling with the proposed approach. Furthermore, our videos presented on the project website illustrate that the generated sequences are smoothly connected to the given partial sequence.



Fig. 3. Text-driven generation results obtained by the *enriched text* task (“from neutral face to bareteeth” (top)), and by the *raw text* task (“angry mouth down” (middle), “disgust high smile” (bottom)). The input texts used for the *raw text* task are the combinations of two terms used for training. For instance, “disgust high smile” is a new description that hasn’t been seen before, which combines “disgust” and “high smile”.

Table 3. Quantitative evaluation of the expression filling task for three different locations of the missing part. Accuracy and FID are computed on the sequences obtained by the mean imputation strategy, and by our diffusion model. Note that accuracy is 83.78% and FID is 2.77 for the ground truth in all cases (FFE, FFM, FFB).

| | Mean Imputation | | Ours | |
|-----|-----------------|-------|--------|------|
| | Acc | FID | Acc | FID |
| FFE | 60.15% | 25.67 | 67.18% | 5.51 |
| FFM | 56.25% | 17.68 | 85.93% | 5.06 |
| FFB | 53.90% | 27.32 | 70.31% | 5.22 |

5.4 Geometry-adaptive generation

We have conducted the geometry-adaptive generation task by using classifier guidance so as to generate a desired facial expression from a given facial anatomy (Alg. 4 of App. D). The BiT used for guidance and the IC used for evaluation are both of type S. \mathcal{S}_K is set to $\{1\}$ if the chosen label is associated with N2E sequences, and to $\{F\}$ otherwise.

Quantitative results are shown in Table 4. The classification accuracy is close to the ground truth, and the visual inspection of the video sequences on the project website shows no gap between the generated frames and the enforced one.

While App. C illustrates the diversity of generated expressions when the model is conditioned on the expression label, we study here the same type of diversity but when the facial geometry of a specific subject is enforced in the conditioning process. To this end, a landmark set L_M has been extracted from a given mesh M . The geometry-adaptive generation task is performed so as to

Table 4. Quantitative evaluation of the geometry-adaptive generation task.

| | Acc | FID |
|-------------------|--------|------|
| Ground truth | 71.01% | 5.57 |
| Geometry-adaptive | 70.43% | 9.26 |

generate a sequence containing L_M , and exhibiting an expression corresponding to a given label y . Then, the generated sequence is retargeted to M with the landmark-guided mesh deformation.

Fig. 4 illustrates the variety of expressions we thus obtained by using a same facial anatomy L_M and a same label y (either “eyebrow” or “high smile”), which confirms that the proposed approach is able to generate expression sequences with sufficient level of diversity, even if a same facial anatomy is used for conditioning.

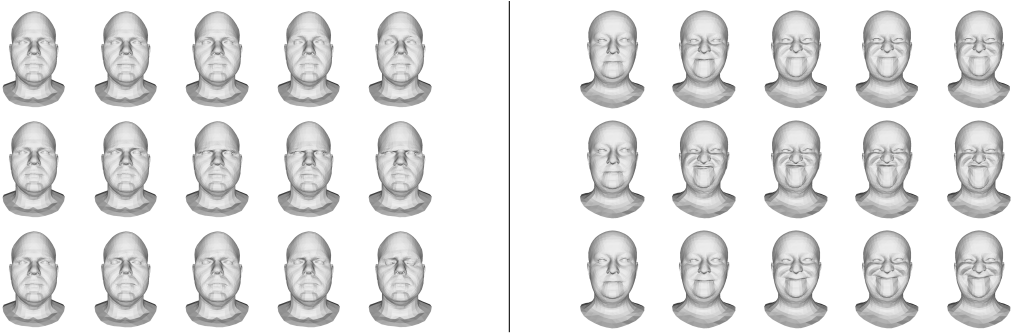


Fig. 4. Diversity of expressions generated with the label “eyebrow” (left), and “high smile” (right) in the geometry-adaptive generation task. All illustrated sequences are of type N2E. Note that eyebrows can be either lowered (the second and third rows) or raised (the first row). Although the poses of maximal expression intensity look all similar in the three sequences of “high smile”, their temporal properties are significantly different. This can be seen more clearly in the video on the project website.

6 RESULTS RELATED TO LANDMARK-GUIDED MESH DEFORMATION

6.1 Comparison with other methods

To the best of our knowledge, only [38] and our work estimate M_f from M and ΔL_f . Note that both approaches use spiral convolution. For the comparative experiments, we also adapt two autoencoders: CoMA [46], which uses Chebyshev convolution and a mesh pooling, and the autoencoder proposed in [4] (the encoder and decoder consisting of three layers of linear, nonlinear, and linear activation units, respectively). Both decoders, which originally take the latent representation of the input mesh as input, have been modified so as to consume the concatenation of the latent representation with ΔL_f .

We conducted two series of experiments: Either 3 expressions (expression split) or 3 subjects (identity split) have been excluded from the training set, and the performance of the model is evaluated on the excluded data. The mean per-vertex Euclidean error between the generated meshes and their ground truth has been measured to assess the performance. Quantitative results are shown in Table 5. While the three methods based on spiral convolution generally yield effective results, our approach outperforms the others, thus confirming the advantage of the cross-attention layer, in particular.

Table 5. Per-vertex reconstruction error (mm).

| Method | Expression split | Identity split |
|---------------------|------------------|-----------------|
| Linear [4] | 0.67 ± 0.76 | 0.73 ± 0.77 |
| CoMA[46] | 0.58 ± 0.63 | 0.63 ± 0.67 |
| S2D [38] | 0.52 ± 0.59 | 0.55 ± 0.62 |
| Ours(w/o attention) | 0.54 ± 0.59 | 0.57 ± 0.64 |
| Ours | 0.45 ± 0.51 | 0.50 ± 0.58 |

We propose to complement our quantitative analysis by a qualitative comparison of the different methods. As the "Expression split" and "Identity split" experiments yield very similar results, we focus solely on the "Identity split" experiment in the following.

Fig. 5 depicts the ground truth mesh (a) as well as the meshes generated with several approaches (b-e). Each vertex of a generated mesh is assigned a color representing the Euclidean distance to its counterpart on the ground truth mesh. As expected, the errors appear mainly on the regions that have been deformed to attain the expression. In Fig. 5, retargeting an expression close to the neutral pose (first row) leads to tiny errors, whereas retargeting an expression "mouth extreme" leads to errors that are mostly located near the mouth. Our approach achieves the best performance in this qualitative error measure, confirming the quantitative results described above.

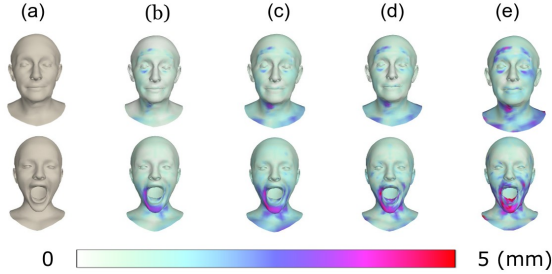


Fig. 5. Qualitative comparison of our method (b) with S2D (c), CoMA (d), and Linear (e) in the landmark-guided deformation of a given mesh. The ground truth meshes are given in the first column (a). The expression of the first row is close to the neutral face and that of the second row is taken from a sequence labeled as "mouth extreme".

6.2 Expression retargeting

Our landmark-guided encoder-decoder can retarget the landmark expression sequences to different facial meshes. In Fig. 6, a landmark sequence generated from our model is used to guide the deformation of three different facial meshes. We can observe that different subjects make the same semantic facial expression in response to the same chosen landmark sequence. As expected, the resulting mesh deformations are well adapted to each facial geometry, which confirms that our model offers the flexibility of combining any desired facial meshes independently from the landmark sequence generation. More results can be found on our project website, where we illustrate the retargeting results of the landmark sequence taken from a full sequence of the CoMA dataset onto several facial meshes.

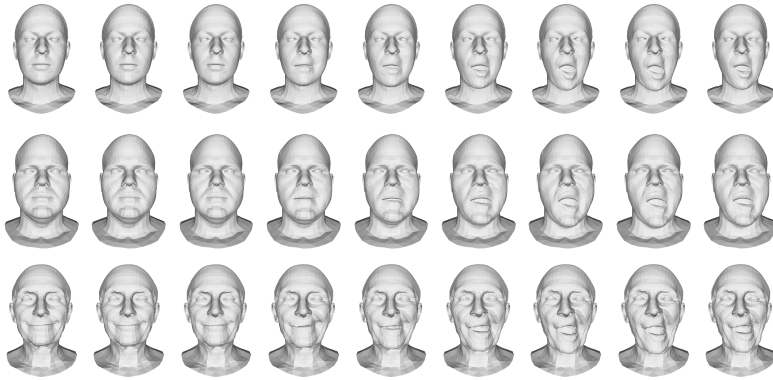


Fig. 6. Expression retargeting results by our landmark-guided encoder-decoder. A same expression sequence (generated by using “mouth side” label) has been applied to three different facial meshes.

7 CONCLUSION

We have presented a generator model to synthesize 3D dynamic facial expressions. The dynamics of facial expressions is first learned unconditionally, from which a series of downstream tasks are developed to synthesize an expression sequence conditioned on various condition signals. Also proposed is a robust face deformation scheme guided by the landmark set, which contributes to a higher reconstruction validity. Experimental results show that the proposed method can produce plausible face meshes of diverse types of expressions on different subjects. In addition, it outperforms SOTA models both qualitatively and quantitatively. As has been demonstrated, our expression generation framework is versatile and can be used in many application scenarios including, but not limited to, label-guided generation, text-driven generation, geometry-adaptive generation, or expression filling.

ACKNOWLEDGMENTS

This work was funded by the TOPACS ANR-19-CE45-0015 project and Human4D ANR-19-CE23-0020 project of the French National Research Agency (ANR).

REFERENCES

- [1] Giorgos Bouritsas, Sergiy Bokhnyak, Stylianos Ploumpis, Michael Bronstein, and Stefanos Zafeiriou. 2019. Neural 3d morphable models: Spiral convolutional networks for 3d shape representation learning and generation. In *Proceedings of the IEEE/CVF International Conference on Computer Vision*. 7213–7222.
- [2] Giorgos Bouritsas, Sergiy Bokhnyak, Stylianos Ploumpis, Michael Bronstein, and Stefanos Zafeiriou. 2019. Neural 3d morphable models: Spiral convolutional networks for 3d shape representation learning and generation. In *Proceedings of the IEEE/CVF International Conference on Computer Vision*. 7213–7222.
- [3] Hamza Bouzid and Lahoucine Ballihi. 2022. Facial Expression Video Generation Based-On Spatio-temporal Convolutional GAN: FEV-GAN. *Intelligent Systems with Applications* (2022), 200139.
- [4] Dan Casas and Miguel A Otaduy. 2018. Learning nonlinear soft-tissue dynamics for interactive avatars. *Proceedings of the ACM on Computer Graphics and Interactive Techniques* 1, 1 (2018), 1–15.
- [5] Shiyang Cheng, Irene Kotsia, Maja Pantic, and Stefanos Zafeiriou. 2018. 4dfab: A large scale 4d database for facial expression analysis and biometric applications. In *Proceedings of the IEEE conference on computer vision and pattern recognition*. 5117–5126.
- [6] Kyunghyun Cho, Bart van Merriënboer, Dzmitry Bahdanau, and Yoshua Bengio. 2014. On the Properties of Neural Machine Translation: Encoder–Decoder Approaches. In *SSST@EMNLP*.
- [7] Darren Cosker, Eva Krumbhuber, and Adrian Hilton. 2011. A FACS valid 3D dynamic action unit database with applications to 3D dynamic morphable facial modeling. In *2011 international conference on computer vision*. IEEE,

2296–2303.

- [8] Yu Deng, Jiaolong Yang, Sicheng Xu, Dong Chen, Yunde Jia, and Xin Tong. 2019. Accurate 3d face reconstruction with weakly-supervised learning: From single image to image set. In *Proceedings of the IEEE/CVF Conference on Computer Vision and Pattern Recognition Workshops*. 0–0.
- [9] Jacob Devlin, Ming-Wei Chang, Kenton Lee, and Kristina Toutanova. 2018. Bert: Pre-training of deep bidirectional transformers for language understanding. *arXiv preprint arXiv:1810.04805* (2018).
- [10] Prafulla Dhariwal and Alexander Nichol. 2021. Diffusion models beat gans on image synthesis. *Advances in Neural Information Processing Systems* 34 (2021), 8780–8794.
- [11] John Duchi, Elad Hazan, and Yoram Singer. 2011. Adaptive subgradient methods for online learning and stochastic optimization. *Journal of machine learning research* 12, 7 (2011).
- [12] Gabriele Fanelli, Juergen Gall, Harald Romsdorfer, Thibaut Weise, and Luc Van Gool. 2010. A 3-d audio-visual corpus of affective communication. *IEEE Transactions on Multimedia* 12, 6 (2010), 591–598.
- [13] Yao Feng, Fan Wu, Xiaohu Shao, Yanfeng Wang, and Xi Zhou. 2018. Joint 3d face reconstruction and dense alignment with position map regression network. In *Proceedings of the European conference on computer vision (ECCV)*. 534–551.
- [14] Claudio Ferrari, Giuseppe Lisanti, Stefano Berretti, and Alberto Del Bimbo. 2017. A dictionary learning-based 3D morphable shape model. *IEEE Transactions on Multimedia* 19, 12 (2017), 2666–2679.
- [15] Ian Goodfellow, Jean Pouget-Abadie, Mehdi Mirza, Bing Xu, David Warde-Farley, Sherjil Ozair, Aaron Courville, and Yoshua Bengio. 2014. Generative adversarial nets. In *Advances in neural information processing systems*. 2672–2680.
- [16] Chuan Guo, Xinxin Zuo, Sen Wang, Shihao Zou, Qingyao Sun, Annan Deng, Minglun Gong, and Li Cheng. 2020. Action2motion: Conditioned generation of 3d human motions. In *Proc. ACM Multimedia*. 2021–2029.
- [17] Jianzhu Guo, Xiangyu Zhu, Yang Yang, Fan Yang, Zhen Lei, and Stan Z Li. 2020. Towards fast, accurate and stable 3d dense face alignment. In *European Conference on Computer Vision*. Springer, 152–168.
- [18] Martin Heusel, Hubert Ramsauer, Thomas Unterthiner, Bernhard Nessler, and Sepp Hochreiter. 2017. Gans trained by a two time-scale update rule converge to a local nash equilibrium. *Advances in neural information processing systems* 30 (2017).
- [19] Jonathan Ho, Ajay Jain, and Pieter Abbeel. 2020. Denoising diffusion probabilistic models. *Advances in Neural Information Processing Systems* 33 (2020), 6840–6851.
- [20] Sepp Hochreiter and Jürgen Schmidhuber. 1997. Long Short-Term Memory. *Neural Computation* 9, 8 (11 1997), 1735–1780. <https://doi.org/10.1162/neco.1997.9.8.1735> arXiv:<https://direct.mit.edu/neco/article-pdf/9/8/1735/813796/neco.1997.9.8.1735.pdf>
- [21] Catalin Ionescu, Dragos Papava, Vlad Olaru, and Cristian Sminchisescu. 2013. Human3.6m: Large scale datasets and predictive methods for 3d human sensing in natural environments. *IEEE transactions on pattern analysis and machine intelligence* 36, 7 (2013), 1325–1339.
- [22] Zi-Hang Jiang, Qianyi Wu, Keyu Chen, and Juyong Zhang. 2019. Disentangled representation learning for 3d face shape. In *Proceedings of the IEEE/CVF Conference on Computer Vision and Pattern Recognition*. 11957–11966.
- [23] Jihoon Kim, Jiseob Kim, and Sungjoon Choi. 2022. Flame: Free-form language-based motion synthesis & editing. *arXiv preprint arXiv:2209.00349* (2022).
- [24] Diederik P Kingma, Shakir Mohamed, Danilo Jimenez Rezende, and Max Welling. 2014. Semi-supervised learning with deep generative models. In *Advances in neural information processing systems*. 3581–3589.
- [25] Diederik P. Kingma and Max Welling. 2014. Auto-Encoding Variational Bayes. In *International Conference on Learning Representations*. <http://arxiv.org/abs/1312.6114>
- [26] Zhifeng Kong, Wei Ping, Jiayi Huang, Kexin Zhao, and Bryan Catanzaro. 2020. Diffwave: A versatile diffusion model for audio synthesis. *arXiv preprint arXiv:2009.09761* (2020).
- [27] Buyu Li, Yongchi Zhao, Shi Zhelun, and Lu Sheng. 2022. Danceformer: Music conditioned 3d dance generation with parametric motion transformer. In *Proceedings of the AAAI Conference on Artificial Intelligence*, Vol. 36. 1272–1279.
- [28] Ruilong Li, Shan Yang, David A Ross, and Angjoo Kanazawa. 2021. Ai choreographer: Music conditioned 3d dance generation with aist++. In *Proceedings of the IEEE/CVF International Conference on Computer Vision*. 13401–13412.
- [29] Tianye Li, Timo Bolkart, Michael J Black, Hao Li, and Javier Romero. 2017. Learning a model of facial shape and expression from 4D scans. *ACM Trans. Graph.* 36, 6 (2017), 194–1.
- [30] Xiang Lisa Li, John Thickstun, Ishaan Gulrajani, Percy Liang, and Tatsunori B Hashimoto. 2022. Diffusion-LM Improves Controllable Text Generation. *arXiv preprint arXiv:2205.14217* (2022).
- [31] Matthew Loper, Naureen Mahmood, Javier Romero, Gerard Pons-Moll, and Michael J Black. 2015. SMPL: A skinned multi-person linear model. *ACM transactions on graphics (TOG)* 34, 6 (2015), 1–16.
- [32] Andreas Lugmayr, Martin Danelljan, Andres Romero, Fisher Yu, Radu Timofte, and Luc Van Gool. 2022. RePaint: Inpainting using Denoising Diffusion Probabilistic Models. In *2022 IEEE/CVF Conference on Computer Vision and Pattern Recognition (CVPR)*. 11451–11461.

- [33] Shitong Luo and Wei Hu. 2021. Diffusion probabilistic models for 3d point cloud generation. In *Proceedings of the IEEE/CVF Conference on Computer Vision and Pattern Recognition*. 2837–2845.
- [34] Naureen Mahmood, Nima Ghorbani, Nikolaus F Troje, Gerard Pons-Moll, and Michael J Black. 2019. AMASS: Archive of motion capture as surface shapes. In *Proceedings of the IEEE/CVF international conference on computer vision*. 5442–5451.
- [35] Alexander Quinn Nichol and Prafulla Dhariwal. 2021. Improved denoising diffusion probabilistic models. In *International Conference on Machine Learning*. PMLR, 8162–8171.
- [36] Naima Otberdout, Mohammed Daoudi, Anis Kacem, Lahoucine Ballihi, and Stefano Berretti. 2020. Dynamic facial expression generation on hilbert hypersphere with conditional wasserstein generative adversarial nets. *IEEE Transactions on Pattern Analysis and Machine Intelligence* (2020).
- [37] Naima Otberdout, Mohammed Daoudi, Anis Kacem, Lahoucine Ballihi, and Stefano Berretti. 2020. Dynamic facial expression generation on hilbert hypersphere with conditional wasserstein generative adversarial nets. *IEEE Transactions on Pattern Analysis and Machine Intelligence* (2020).
- [38] Naima Otberdout, Claudio Ferrari, Mohamed Daoudi, Stefano Berretti, and Alberto Del Bimbo. 2022. Sparse to Dense Dynamic 3D Facial Expression Generation. In *Proceedings of the IEEE/CVF Conference on Computer Vision and Pattern Recognition*. 20385–20394.
- [39] Mathis Petrovich, Michael J Black, and Gül Varol. 2021. Action-conditioned 3d human motion synthesis with transformer vae. In *Proceedings of the IEEE/CVF International Conference on Computer Vision*. 10985–10995.
- [40] Matthias Plappert, Christian Mandery, and Tamim Asfour. 2016. The KIT motion-language dataset. *Big data* 4, 4 (2016), 236–252.
- [41] Rolandos Alexandros Potamias, Jiali Zheng, Stylianos Ploumpis, Giorgos Bouritsas, Evangelos Ververas, and Stefanos Zafeiriou. 2020. Learning to Generate Customized Dynamic 3D Facial Expressions. In *Computer Vision – ECCV 2020: 16th European Conference* (Glasgow, United Kingdom). Springer-Verlag, 278–294. https://doi.org/10.1007/978-3-030-58526-6_17
- [42] Abhinanda R Punnakkal, Arjun Chandrasekaran, Nikos Athanasiou, Alejandra Quiros-Ramirez, and Michael J Black. 2021. BABEL: Bodies, action and behavior with english labels. In *Proceedings of the IEEE/CVF Conference on Computer Vision and Pattern Recognition*. 722–731.
- [43] Alec Radford, Jong Wook Kim, Chris Hallacy, Aditya Ramesh, Gabriel Goh, Sandhini Agarwal, Girish Sastry, Amanda Askell, Pamela Mishkin, Jack Clark, et al. 2021. Learning transferable visual models from natural language supervision. In *International Conference on Machine Learning*. PMLR, 8748–8763.
- [44] Aditya Ramesh, Prafulla Dhariwal, Alex Nichol, Casey Chu, and Mark Chen. 2022. Hierarchical text-conditional image generation with clip latents. *arXiv preprint arXiv:2204.06125* (2022).
- [45] Anurag Ranjan, Timo Bolkart, Soubhik Sanyal, and Michael J Black. 2018. Generating 3D faces using convolutional mesh autoencoders. In *Proceedings of the European conference on computer vision (ECCV)*. 704–720.
- [46] Anurag Ranjan, Timo Bolkart, Soubhik Sanyal, and Michael J Black. 2018. Generating 3D faces using convolutional mesh autoencoders. In *Proceedings of the European conference on computer vision (ECCV)*. 704–720.
- [47] Danilo Rezende and Shakir Mohamed. 2015. Variational inference with normalizing flows. In *International conference on machine learning*. PMLR, 1530–1538.
- [48] Robin Rombach, Andreas Blattmann, Dominik Lorenz, Patrick Esser, and Björn Ommer. 2022. High-resolution image synthesis with latent diffusion models. In *Proceedings of the IEEE/CVF Conference on Computer Vision and Pattern Recognition*. 10684–10695.
- [49] Olaf Ronneberger, Philipp Fischer, and Thomas Brox. 2015. U-net: Convolutional networks for biomedical image segmentation. In *International Conference on Medical image computing and computer-assisted intervention*. Springer, 234–241.
- [50] Chitwan Saharia, William Chan, Saurabh Saxena, Lala Li, Jay Whang, Emily Denton, Seyed Kamyar Seyed Ghasemipour, Burcu Karagol Ayan, S Sara Mahdavi, Rapha Gontijo Lopes, et al. 2022. Photorealistic Text-to-Image Diffusion Models with Deep Language Understanding. *arXiv preprint arXiv:2205.11487* (2022).
- [51] Hyewon Seo and Guoliang Luo. 2021. Generating 3D Facial Expressions with Recurrent Neural Networks. In *Intelligent Scene Modeling and Human-Computer Interaction*. Springer International Publishing, 181–196. https://doi.org/10.1007/978-3-030-71002-6_11
- [52] Jascha Sohl-Dickstein, Eric Weiss, Niru Maheswaranathan, and Surya Ganguli. 2015. Deep unsupervised learning using nonequilibrium thermodynamics. In *International Conference on Machine Learning*. PMLR, 2256–2265.
- [53] Yang Song, Jascha Sohl-Dickstein, Diederik P Kingma, Abhishek Kumar, Stefano Ermon, and Ben Poole. 2020. Score-based generative modeling through stochastic differential equations. *arXiv preprint arXiv:2011.13456* (2020).
- [54] Guy Tevet, Brian Gordon, Amir Hertz, Amit H Bermano, and Daniel Cohen-Or. 2022. MotionCLIP: Exposing Human Motion Generation to CLIP Space. *arXiv preprint arXiv:2203.08063* (2022).
- [55] Guy Tevet, Sigal Raab, Brian Gordon, Yonatan Shafir, Daniel Cohen-Or, and Amit H Bermano. 2022. Human Motion Diffusion Model. *arXiv preprint arXiv:2209.14916* (2022).

- [56] Xiaoguang Tu, Jian Zhao, Mei Xie, Zihang Jiang, Akshaya Balamurugan, Yao Luo, Yang Zhao, Lingxiao He, Zheng Ma, and Jiashi Feng. 2020. 3D face reconstruction from a single image assisted by 2D face images in the wild. *IEEE Transactions on Multimedia* 23 (2020), 1160–1172.
- [57] Sergey Tulyakov, Ming-Yu Liu, Xiaodong Yang, and Jan Kautz. 2018. MoCoGAN: Decomposing Motion and Content for Video Generation. In *2018 IEEE/CVF Conference on Computer Vision and Pattern Recognition*. 1526–1535. <https://doi.org/10.1109/CVPR.2018.00165>
- [58] Ashish Vaswani, Noam Shazeer, Niki Parmar, Jakob Uszkoreit, Llion Jones, Aidan N Gomez, Lukasz Kaiser, and Illia Polosukhin. 2017. Attention is all you need. In *Advances in neural information processing systems*. 5998–6008.
- [59] Wei Wang, Xavier Alameda-Pineda, Dan Xu, Pascal Fua, Elisa Ricci, and Nicu Sebe. 2018. Every smile is unique: Landmark-guided diverse smile generation. In *Proc. IEEE Conference on Computer Vision and Pattern Recognition*. 7083–7092.
- [60] Yaohui Wang, Piotr Bilinski, Francois Bremond, and Antitza Dantcheva. 2020. G3AN: Disentangling Appearance and Motion for Video Generation. In *IEEE/CVF Conference on Computer Vision and Pattern Recognition*.
- [61] Yaohui Wang, Piotr Bilinski, Francois Bremond, and Antitza Dantcheva. 2020. Imaginator: Conditional spatio-temporal gan for video generation. In *Proceedings of the IEEE/CVF Winter Conference on Applications of Computer Vision*. 1160–1169.
- [62] Mingyuan Zhang, Zhongang Cai, Liang Pan, Fangzhou Hong, Xinying Guo, Lei Yang, and Ziwei Liu. 2022. Motiondiffuse: Text-driven human motion generation with diffusion model. *arXiv preprint arXiv:2208.15001* (2022).
- [63] Xing Zhang, Lijun Yin, Jeffrey F Cohn, Shaun Canavan, Michael Reale, Andy Horowitz, and Peng Liu. 2013. A high-resolution spontaneous 3d dynamic facial expression database. In *IEEE workshops on automatic face and gesture recognition*. 1–6.

A ADVANTAGE OF USING A BIDIRECTIONAL TRANSFORMER

In order to efficiently capture the temporal features of x_t , we use a bidirectional Transformer (BiT) as the noise approximator as well as the classifier used for the guidance. We compare the performance of the bidirectional Transformer to other popular neural networks such as Transformer [58] and U-Net [49], the most frequently used model for 2D images.

We use a 1D U-Net that takes as input a tensor of size $channels=40$ and $num_features=68 \times 3$, where 40 is the sequence length, and 68 the number of 3D landmarks. These models are evaluated in the context of the label control task on the CoMA dataset, as detailed in Sec. 5.1. Results are given in Tab. 6.

Table 6. Quantitative evaluation of the label control task. The noise approximator and the classifier used for the guidance are modeled either with a U-Net, a Transformer, or a BiT.

| Model | Accuracy | FID |
|-------------|----------|-------|
| U-Net | 50.04% | 21.36 |
| Transformer | 80.29% | 7.57 |
| BiT | 84.97% | 6.79 |

As expected, U-Net is not adapted to temporal sequence modeling. We observe that the best results are obtained by using a BiT.

B TRAINING WITH SEQUENCES OF ANY LENGTH AND GENERATION OF SEQUENCES OF ARBITRARY LENGTH

Since our noise approximator is a bidirectional transformer, it can take sequences of any length as input —It can be trained using sequences of any length, and we can sample from the resulting model so as to obtain sequences of desired lengths (The length of x_0 will be that of x_T). In the same way, as a bidirectional transformer is used also to guide the reverse process, it can guide the reverse process with any length for x_t . Consequently, tasks related to label control, text control, and geometry-adaptive generation can generate sequences of any desired length. Furthermore, the sequences that have to be filled with the expression filling task can be of any length.

For the sake of simplicity, we describe here only the label control task. The noise approximator and the classifier used for the guidance are either trained using sequences of a fixed length ($F = 40$) or variable lengths (F is uniformly distributed in the interval $[35, 45]$).

The performance of both models is evaluated when outputting sequences of length in $[35, 45]$. The performance is evaluated as in Sec. 5.1, except that the independent classifier is trained with sequences of variable length (F is uniformly distributed in $[35, 45]$). Results are shown in Fig.??.

When generating sequences of different lengths is required, training with variable lengths helps the model to perform better. Moreover, the results obtained with the model trained with sequences of variable length are satisfactory: the achieved accuracy is similar to that of the ground truth. Moreover, the FID obtained for a length frame of 40 is similar to that calculated with the model dedicated to output sequences of length 40.

C DIVERSITY OF THE GENERATED SEQUENCES WHEN CONDITIONING ON EXPRESSION LABEL

We study in this section the diversity of the generated sequences both in terms of facial anatomy (L) and in terms of expression (ΔL_f) in the label control task. As a reminder, the 3D arrangement of

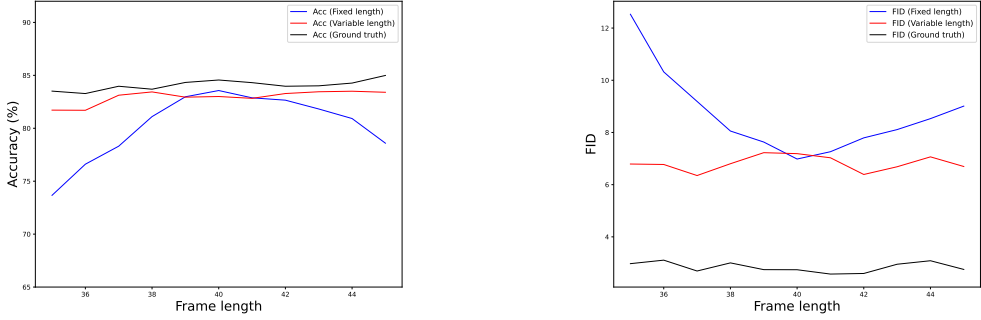


Fig. 7. Quantitative evaluation of the label control task for models trained with sequences of a fixed length ($F = 40$) or variable lengths. Performance is evaluated on generated sequences of different lengths using, as in Sec. 5.1, the classification accuracy (left) and the FID score (right).

a landmark frame L_f can be regarded as the combination of the facial anatomy (at a neutral pose L) and the expression-driven shape change applied to it, i.e. $L_f = \Delta L_f + L$.

Since the proposed landmark-guided mesh deformation retargets the expression $\Delta L_f = L_f - L$ onto a new face anatomy given as a mesh M , it is used hereafter to illustrate the diversity of the generated expressions but it is not adapted to analyze the facial anatomy of the generated L . To show the diversity of facial anatomy generated by our model, we use the FLAME model[29] to compute the facial mesh from the landmark set of neutral pose¹.

Fig. 8 presents three illustrative neutral faces L that we generated by conditioning the reverse process on the same expression label “mouth open”. Both landmark set and the FLAME-fitted mesh are shown, for each face. (The neutral face L associated with a generated sequence x_0 is set to either L_1 or L_F , depending on the sequence type.) Additionally, the diversity in the generated expression is illustrated in Fig. 9. The apparent distinction among these results demonstrate that the proposed approach is able to generate sequences of rich diversity, both in terms of facial anatomy and expression (This is due to the input noise x_T that is sampled from $\mathcal{N}(0, I)$).

¹We can note that the meshes generated from FLAME lack certain details of the facial geometry, resulting in dull, lifeless shapes. Furthermore, FLAME takes about 470s to fit one sequence, while the proposed landmark-guided mesh deformation needs only about 1.30s.

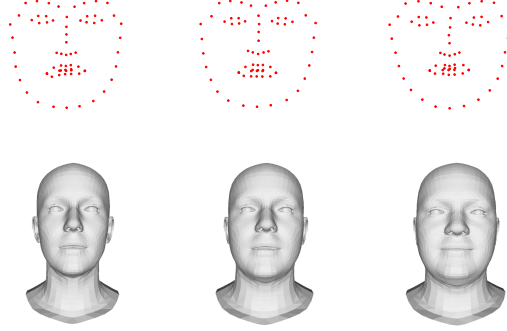


Fig. 8. Diversity of facial anatomy in the generated expressions. We use FLAME model to compute facial meshes from the landmark sets, for the visualization purpose.

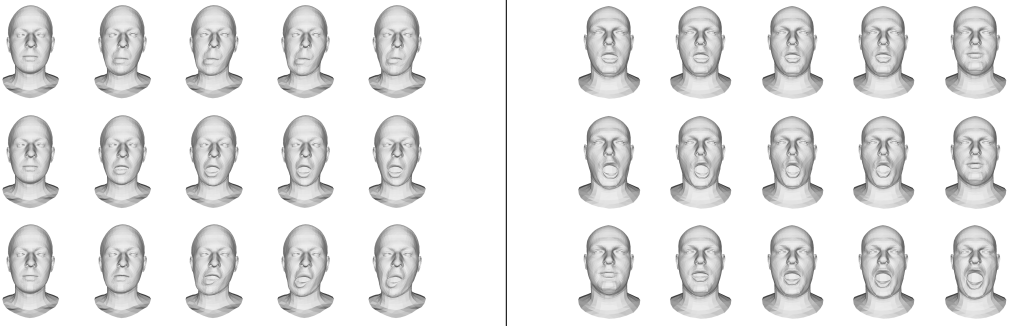


Fig. 9. Diversity of expressions generated with the label “mouth side” (left), and “mouth open” (right) in the label control task. Note that generated sequences can be either of type E2N or N2E.

D PSEUDO CODE FOR EACH DOWNSTREAM TASK

Algorithm 1 Label control

Input: Label y .

Output: Sequence x_0 (corresponding to label y).

- 1: $x_T \sim N(0, I)$
 - 2: **for** $t = T, \dots, 1$ **do**
 - 3: ▷ Estimation of $p_\theta(\cdot|x_t)$
 - 4: Compute $\epsilon_\theta(x_t, t)$
 - 5: Compute $\mu_\theta(x_t, t): \mu_\theta(x_t, t) = \frac{1}{\sqrt{\alpha_t}} \left(x_t - \frac{\beta_t}{\sqrt{1-\alpha_t}} \epsilon_\theta(x_t, t) \right)$
 - 6: ▷ Sampling from $p_\theta(\cdot|x_t)$
 - 7: $z \sim N(0, I)$ if $t > 1$, 0 otherwise
 - 8: Set \hat{x}_{t-1} to $\mu_\theta(x_t, t) + \sigma_t z$
 - 9: ▷ Optimization: optimization procedure is initialized with \hat{x}_{t-1}
 - 10: $x_{t-1} = \underset{x}{\operatorname{argmax}} \left[\lambda \log(p_\theta(x|x_t)) + \log(p_\phi(y|x, t-1)) \right]$
- return** x_0
-

Algorithm 2 Text control**Input:** Text c .**Output:** Sequence x_0 (corresponding to text c).

```

1:  $x_T \sim N(0, I)$ 
2: for  $t = T, \dots, 1$  do
3:                                      $\triangleright$  Estimation of  $p_\theta(\cdot|x_t)$ 
4:   Compute  $\epsilon_\theta(x_t, t)$ 
5:   Compute  $\mu_\theta(x_t, t): \mu_\theta(x_t, t) = \frac{1}{\sqrt{\alpha_t}} \left( x_t - \frac{\beta_t}{\sqrt{1-\alpha_t}} \epsilon_\theta(x_t, t) \right)$ 
6:                                      $\triangleright$  Sampling from  $p_\theta(\cdot|x_t)$ 
7:    $z \sim N(0, I)$  if  $t > 1$ , 0 otherwise
8:   Set  $\hat{x}_{t-1}$  to  $\mu_\theta(x_t, t) + \sigma_t z$ 
9:                                      $\triangleright$  Optimization: optimization procedure is initialized with  $\hat{x}_{t-1}$ 
10:   $x_{t-1} = \underset{x}{\operatorname{argmax}} [\lambda \log(p_\theta(x|x_t)) + \cos(\text{BiT}(x, t-1), \text{CLIP}(c))]$ 
return  $x_0$ 

```

Algorithm 3 Sequence filling**Input:** Partial sequence $x_0|_{S_K}$ **Output:** Completed sequence x_0

```

1:  $x_T|_{S_U} \sim N(0, I)$ 
2:  $x_T|_{S_K} = \sqrt{\bar{\alpha}_T} x_0|_{S_K} + \sqrt{1-\bar{\alpha}_T} \epsilon, \epsilon \sim N(0, I)$ 
3: for  $t = T, \dots, 1$  do
4:                                      $\triangleright$  Estimation of  $p_\theta(\cdot|x_t)$ 
5:   Compute  $\epsilon_\theta(x_t, t)$ 
6:   Compute  $\mu_\theta(x_t, t): \mu_\theta(x_t, t) = \frac{1}{\sqrt{\alpha_t}} \left( x_t - \frac{\beta_t}{\sqrt{1-\alpha_t}} \epsilon_\theta(x_t, t) \right)$ 
7:                                      $\triangleright$  Sampling from  $p_\theta(\cdot|x_t)$ 
8:    $z \sim N(0, I)$  if  $t > 1$ , 0 otherwise
9:   Set  $\hat{x}_{t-1}$  to  $\mu_\theta(x_t, t) + \sigma_t z$ 
10:                                      $\triangleright$  Computation of  $x_{t-1}$ 
11:   $x_{t-1}|_{S_U} = \hat{x}_{t-1}|_{S_U}$ 
12:  if  $t > 1$  then  $\triangleright$  if  $t = 1$ ,  $x_0|_{S_K}$  is already properly set.
13:     $x_{t-1}|_{S_K} = \sqrt{\bar{\alpha}_{t-1}} x_0|_{S_K} + \sqrt{1-\bar{\alpha}_{t-1}} \epsilon, \epsilon \sim N(0, I)$ 
return  $x_0$ 

```

Algorithm 4 Geometry-adaptive generation with label control

Input: Label y and partial sequence $x_0|_{S_K}$. S_K is either $\{1\}$ or $\{F\}$ and the unique frame associated with $x_0|_{S_K}$ is a neutral one.

Output: Completed sequence x_0 (corresponding to label y)

```

1: for  $i = 1$  to 5 do
2:   if  $i == 1$  then
3:      $x_T|_{S_U} \sim N(0, I)$ 
4:      $x_T|_{S_K} = \sqrt{\bar{\alpha}_T}x_0|_{S_K} + \sqrt{1 - \bar{\alpha}_T}\epsilon, \epsilon \sim N(0, I)$ 
5:   else
6:      $x_T = \sqrt{\bar{\alpha}_T}x_0 + \sqrt{1 - \bar{\alpha}_T}\epsilon, \epsilon \sim N(0, I)$ 
7:   for  $t = T, \dots, 1$  do
8:     ▷ Estimation of  $p_\theta(\cdot|x_t)$ 
9:     Compute  $\epsilon_\theta(x_t, t)$ 
10:    Compute  $\mu_\theta(x_t, t): \mu_\theta(x_t, t) = \frac{1}{\sqrt{\alpha_t}} \left( x_t - \frac{\beta_t}{\sqrt{1 - \alpha_t}} \epsilon_\theta(x_t, t) \right)$ 
11:    ▷ Sampling from  $p_\theta(\cdot|x_t)$ 
12:     $z \sim N(0, I)$  if  $t > 1$ , 0 otherwise
13:    Set  $\hat{x}_{t-1}$  to  $\mu_\theta(x_t, t) + \sigma_t z$ 
14:    ▷ Optimization: optimization procedure is initialized with  $\hat{x}_{t-1}$ 
15:     $\hat{x}_{t-1} = \underset{x}{\operatorname{argmax}} \left[ \lambda \log(p_\theta(x|x_t)) + \log(p_\phi(y|x, t-1)) \right]$ 
16:    ▷ Computation of  $x_{t-1}$ 
17:     $x_{t-1}|_{S_U} = \hat{x}_{t-1}|_{S_U}$ 
18:    if  $t > 1$  then ▷ if  $t = 1$ ,  $x_0|_{S_K}$  is already properly set.
19:       $x_{t-1}|_{S_K} = \sqrt{\bar{\alpha}_{t-1}}x_0|_{S_K} + \sqrt{1 - \bar{\alpha}_{t-1}}\epsilon, \epsilon \sim N(0, I)$ 
return  $x_0$ 

```
